*Friction* **2**(4): 295–309 (2014)
DOI 10.1007/s40544-014-0070-2
ISSN 2223-7690
CN 10-1237/TH

**REVIEW ARTICLE**

# Underwater drag reduction by gas

**Jiadao WANG*, Bao WANG, Darong CHEN**

*State Key Laboratory of Tribology, Tsinghua University, Beijing 100084, China*

*Received: 26 October 2014 / Revised: 28 November 2014 / Accepted: 02 December 2014*



**Abstract:** Publications on underwater drag reduction by gas have been gathered in the present study. Experimental methods, results and conclusions from the publications have been discussed and analyzed. The stable existence of gas is a requirement for underwater drag reduction induced by slippage at the water–solid interface. A superhydrophobic surface can entrap gas in surface structures at the water–solid interface. However, many experimental results have exhibited that the entrapped gas can disappear, and the drag gradually increases until the loss of drag reduction with immersion time and underwater flow. Although some other surface structures were also experimented to hold the entrapped gas, from the analysis of thermodynamics and mechanics, it is difficult to prohibit the removal of entrapped gas in underwater surface structures. Therefore, it is essential to replenish a new gas supply for continued presence of gas at the interface for continued underwater drag reduction. Active gas supplement is an effective method for underwater drag reduction, however, that needs some specific equipment and additional energy to generate gas, which limits its practical application. Cavitation or supercavitation is a method for passive gas generation, but it is only adaptive to certain vehicles with high speed. Lately, even at low speed, the evaporation induced by liquid–gas–solid interface of a transverse microgrooved surface for continued gas supply has been discovered, which should be a promising method for practical application of underwater drag reduction by gas.

**Keywords:** drag reduction; entrapped gas; skin friction; underwater

## 1 Introduction

Drag reduction is essential for vehicles on water or underwater to increase voyage and voyaging speed and decrease energy consumption, thermal damage, and noise. In general, a vehicle drag is composed of a pressure or form drag, wave-making resistance, and skin drag. The previous two mainly depend on body's shape, and the latter one on the fluid–solid interface. The pressure drag and the wave making resistance mainly accounts for the total drag of blunt-nosed bodies and high-speed surface ships respectively. However, for streamlined bodies, skin drag represents the largest percentage, even over 60% or 80% in air or underwater and 100% for pipe transportation [1, 2]. Therefore, skin drag is the key for the drag reduction of a streamlined body.

Studies on skin drag reduction have attracted attentions due to their practical value in engineering applications [3, 4]. The skin drag is caused by viscous drag in a boundary layer of fluid around a body. The boundary layer is in the immediate vicinity of a bounding surface, and can be divided into three types of sub-layers, i.e., laminar, buffer, and turbulent, from the wall into the flow [5]. In the turbulent sub-layer, unsteady vortices appear on many scales and interact with each other, causing skin drag increase. Up to now, many theoretical and experimental investigations have been conducted to modify the turbulent structure for drag reduction [6, 7], such as microstructured surface [8–12], polymeric additives [13–16], and traveling wave [17]. Velocity gradient reduction is a reason for the decrease in skin friction drag [18–27]. Therefore, the turbulent sub-layer is normally selected to enlarge

* Corresponding author: Jiadao WANG.
E-mail: jdwang@mail.tsinghua.edu.cn

the thickness of boundary layer to decline the velocity gradient. Based on the investigation of shark scales, the longitudinal grooves (riblets) can be considered as a typical method to reduce the velocity gradient by affecting turbulent sub-layer structure. The height of riblets is several hundreds of micrometers, which is sufficient to affect the structure of turbulent layer [8, 18]. In addition, traveling waves can be used to modify the turbulent sub-layer structure for drag reduction, whose wave structures are vertical with flow direction and larger than riblets [8, 18]. However, when the structure in the turbulent sub-layer is modified, additional energy is essential to enhance the thickness of boundary layer due to energy dissipation in turbulent flow. Therefore, the drag reduction by modifying the structure of the turbulent sub-layer is limited. Various riblets and wave structures have been investigated, and a drag reduction rate of approximately 10% has been achieved [18–27].

Except modifying the turbulent structure of boundary layers, a transverse microgrooved structure has been proposed to achieve non-zero velocity at the same surface height to reduce the velocity gradient in laminar sub-layer near the solid surface for drag reduction [5]. When a liquid flows over the transverse microgrooved surface, vortexes can be formed in microgrooves, and on the upside of the vortex, the revolving direction is consistent with the main flow, which induces the flow shear rate reduction, as shown in Fig. 1. In this method, the scale of microgrooves is less than the thickness of laminar sub-layer. A drag reduction rate of 10% or more was achieved by a transverse microgrooved surface [5].

The above methods for drag reduction, by influencing boundary layer using riblets or other surface structures, can be applied in air or water [23, 28–31]. However, for an underwater vehicle, a gas lubricating

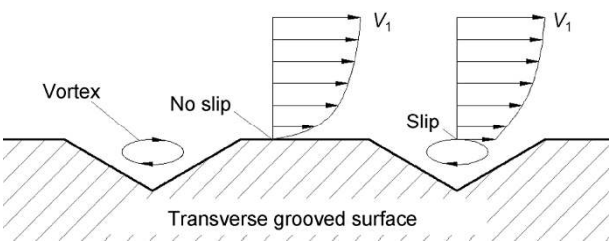


**Fig. 1** Velocity profile on transverse microgrooved surface in flowing water [5].

film on the solid surface can achieve much more effective drag reduction aided by significantly small viscosity of gas compared to water. Recently, several approaches, such as entrapped gas within superhydrophobic surfaces [32–34], gas injection [35], gas generation by electric field or heating [36], and gas generation induced by three-phase interface [37], have been suggested to achieve a gas layer on a surface. In this study, major achievements of underwater drag reduction by gas for 20 years have been gathered and analyzed, and critical points to achieve viable underwater drag reduction are proposed.

## 2 Entrapped gas underwater

When free gas bubbles are formed in water, the pressure in bubbles is higher than that in liquid because of the Laplace pressure of the water–gas interface, resulting in the diffusion and disappearance of gas in the bubbles under the gas solubility limit [38]. Even when the gas solubility limit exceeds, since the Laplace pressure is higher around the smaller free bubbles, gas will diffuse from smaller to larger bubbles through Ostwald Ripening. Large free bubbles will eventually separate from water because of buoyancy. Therefore, free gas bubbles cannot stably exist in water [38–41].

However, when a gas bubble is entrapped at a water-solid interface underwater, especially at a crack or a concave of a hydrophobic solid surface (Fig. 2), the results will be different [38–41]. At thermodynamic equilibrium, thermodynamics and Laplace pressure of the meniscus interface illustrate that the curvature of the concave meniscus interface ($1/r_1 + 1/r_2$) is related to the relative gas concentration, as shown in Eq. (1), which is similar to the Kelvin equation:

$$r_{\mathrm{k}} = \left(\frac{1}{r_1} + \frac{1}{r_2}\right)^{-1} = \frac{\gamma v}{kT\log\left(c/s\right)} \tag{1}$$

where $r_{\mathrm{k}}$ is the equilibrium radius, $v$ is the molecular volume, $\gamma$ is the interface tension, $s$ is the gas concentration in water near the interface, and $c$ is the gas solubility limit. From Eq. (1) and Fig. 2, entrapped gas can stably exist even under the gas solubility limit when the equilibrium radius $r_{\mathrm{k}}$ is larger than the minimal radius of the concave $r_{\mathrm{c}}$.

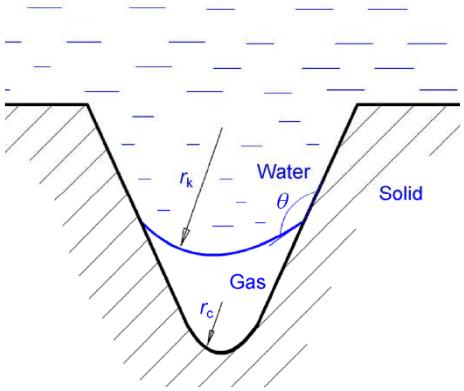


**Fig. 2** Entrapped gas at a concave of an underwater solid interface.

As per Eq. (1), $r_k$ is always larger than zero when $s$ is less than $c$. Therefore, in terms of thermodynamics, under the gas solubility limit, gas cannot exist at a flat solid–liquid interface. However, some experimental evidences have been presented for the existence of nanosized gas at a flat solid–liquid interface and some reasons have been analyzed [38–42].

### 2.1 Existence of nanosized gas at the solid–liquid interface

Recently, there has been an accumulation of evidences for the existence of nanobubbles on flat hydrophobic surfaces in water regardless of predictions that such small bubbles should rapidly dissolve because of the high internal pressure associated with the interfacial curvature [38, 39]. The reason for existence of nanobubble on a flat surface has been investigated. Figure 3 shows that the contact angle of a nanosized bubble is much larger than the macroscopic contact angle on the same substrate resulting in a larger radius of curvature and a proportionate decrease in the Laplace pressure [40]; therefore increasing the lifetime of the nanosized gas. There is a minute difference in the inside and outside gas pressure of air bubbles, leading to a slight chemical potential difference across the interface [41, 42]. Though the above analysis is applicable for the existence of nanobubbles on an underwater flat surface, a further thermodynamic investigation is required in near future.

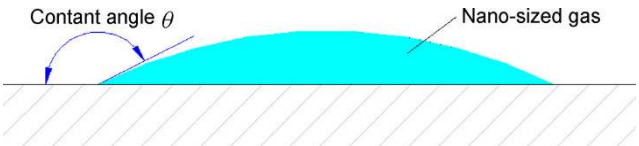


**Fig. 3** Nanosized gas at water−solid interface.

### 2.2 Existence of entrapped gas in surface structures

For a more effective underwater drag reduction, high gas coverage percentage on a surface is expected. Based on the analysis of Eq. (1) and Section 2.1, it is difficult for large gas bubbles to exist stably on an underwater flat surface. Many studies have shown that large gas bubbles can exist in the microstructures of a surface [41, 42]. A superhydrophobic surface is a typical one with microstructures entrapping gas under a water drop. Superhydrophobicity originates from the self-cleaning characteristics of the leaves of plants, notably the lotus leaf [43]. Thereafter, many fabrication methods have been presented through the imitation of natural superhydrophobic surfaces and mechanism of superhydrophobicity has been investigated [44–46].

#### *2.2.1 Entrapped gas in superhydrophobic surface structures*

Nature is an inspiration for many innovations and continues to serve as a valuable resource to solve technical challenges [47–49]. Superhydrophobic surfaces, with a large apparent contact angle and a small contact angle hysteresis, were originally inspired by the unique water-repellent property of lotus and rice leaves and butterfly wings [50–55]. For a superhydrophobic surface, water droplets roll-off faster than other surfaces. This behavior is explained by the reduction of contact area between the surface and water, which indicates that the gas can be sustained in surface topography under a droplet to change the macroscopic boundary condition to allow non-zero slip velocity [56]. In general, a water drop on a rough surface spreads and immerses the surface topography; this state is called the Wenzel state with a large contact angle hysteresis [57]. However, sometimes, the drop is suspended above the surface topography, entrapping gas between the drop and surface, called the Cassie state, resulting in the superhydrophobic behavior of the drop on the surface [58]. Superhydrophobic surfaces have the potential to reduce hydrodynamic drag by combining a structured surface and hydrophobicity to retain a lubricating air layer (plastron) at the surface [59]. There are many superhydrophobic surfaces such as lotus, rice, and taro leaves. As

shown in Fig. 4, entrapped gas can be observed when a lotus leaf is immersed in water. Among diverse nature of superhydrophobic surfaces, one typical character is that the surface topography is mainly composed of homogeneous one or multiscale papilla on a lotus leaf (Fig. 5) [43].

Based on investigations, several methods have been developed to fabricate superhydrophobic surfaces, such as microwave plasma-enhanced chemical vapor deposition [23] of trimethylmethoxysilane treatment [13], template method [11], spraying or dipping [12], laser and plasma process [19], and chemical plating [26]. The obtained images indicated that the artificial bionic superhydrophobic surfaces could sustain gas under a water drop [60]. The existence of entrapped gas has drawn much attention for underwater drag reduction. When the superhydrophobic surfaces were immersed in water and viewed at a glancing angle, they appeared as a silver mirror [61]. Because of reflection at the liquid–gas interface on the superhydrophobic surface, optical observations of the underwater gas phase were usually used in the investigation of entrapped gas within surfaces in liquid [61–64]. Besides the optical visualization of gas, the profile of the water–gas interface obtained by atomic force microscope on the superhydrophobic surface underwater was employed. In addition, a small angle X-ray scattering method was applied to investigate the entrapped gas in the microstructures of a superhydrophobic surface [65]. Both the theoretical and experimental results depicted that superhydrophobic surfaces can sustain gas within underwater surfaces.

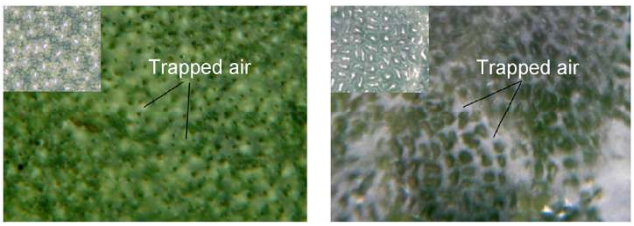


**Fig. 4** Trapped gas on a lotus leaf in water [43].

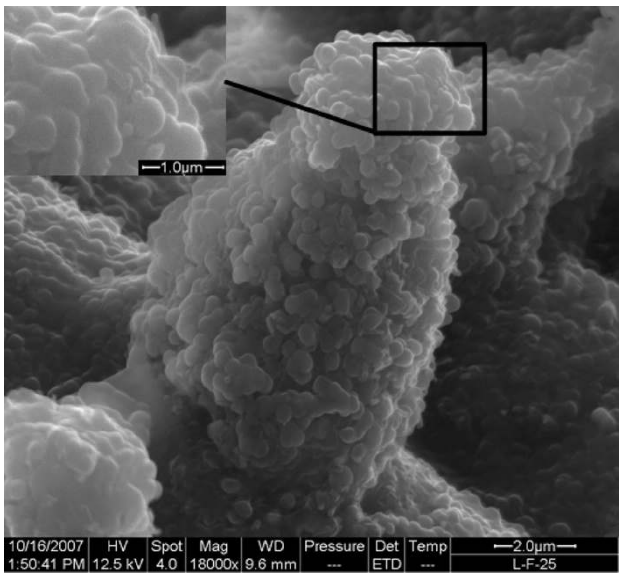


**Fig. 5** Scanning electron microscope (SEM) image of a lotus leaf surface [43].

### 2.2.2 *Mechanical criteria for the existence of entrapped gas*

The existence of entrapped gas in surface structures is a necessary condition for the superhydrophobicity of diverse surfaces. The superhydrophobicity of a surface, biomimicking from natural leaves, is determined by its chemical composition and topography. The surface chemical compositions of the wax-like materials covering plant leaves provide low surface free energy. The surface structures play a critical role for superhydrophobicity because of main responsibility for the existence of the entrapped gas.

In general, the larger the fractional solid–gas interface area induced by the entrapped gas, the more hydrophobic is the surface. For a superhydrophobic surface, such as with regular distributed pillars, the solid–water contact area is minimized; therefore, the gas coverage under a drop on the surface is enlarged. However, when the fractional solid–gas interface area becomes very large, the liquid intrudes into the underlying solid between asperities [44–46]. Therefore, the key for superhydrophobic surface design is to entrap gas in the microstructures of a surface or prohibit the transition from the Cassie to Wenzel state. Many investigators have focused on the relation between the entrapped gas under a drop and surface geometry, including pillar height, diameter, top perimeter, overall filling factor, and disposition [66, 67]. Barbieri et al. [44] presented a criterion on an energy barrier achieved from the surface energy variation between the Cassie and Wenzel states based on energy analysis to evaluate the state of superhydrophobic surface. Extrand [45] proposed a contact line density criterion based on the balance between the weight of

unsupported liquid and the surface tension at the three-phase contact line. In the criterion, a critical value of contact line density was quantitatively provided, which can be easily used to evaluate a superhydrophobic surface. Wang and Chen [46] proposed an intruding angle criterion for the design of a superhydrophobic surface. The intruding angle can be described as follows:

$$\beta = \pi - \theta_0 + \arcsin\left\{\frac{f_{LG}}{\lambda}\frac{1}{\sigma}\left[\frac{2\sigma}{R_D} + \rho g R_D(1-\cos\theta)\right]\right\} \quad (2)$$

where $\theta_0$ is the contact angle on a flat surface, $f_{LG}$ is the ratio of the projected area of the liquid–gas interface to the apparent contact area under the droplet, $\lambda$ is the contact line density, i.e., the length of contact line over the entrapped gas per unit apparent contact area, $2\sigma/R_D$ is the pressure induced by the surface tension at the apex of the droplet, $R_D$ is the radius of the droplet, and $\theta$ is the apparent contact angle.

According to the intruding angle criterion deduced from the force equilibrium of the interfaces under the drop, the interfacial forces under the drop must be of sufficient magnitude to suspend the drop against the downward pull of gravity to avoid the water intruding into surface structures. When a calculated intruding angle from the measured parameters is less than the asperity angle, the water drop suspends on the surface structures or else the water intrudes into surface structures. Though the intruding angle criterion was deduced for a pillar surface structure, it can also be used for a concave surface structure. Besides the intruding angle criterion, an intruding depth criterion is specified for superhydrophobic surface design; as per that, asperities must be sufficiently tall to prevent the water from contacting the underlying solid [46]. When Eq. (2) is applied for evaluating the entrapped gas of a submerged underwater surface, it can be modified as follows:

$$\beta = \pi - \theta_0 + \arcsin\left\{\frac{f_{LG}}{\lambda}\frac{1}{\sigma}\left(P_L - P_G\right)\right\} \quad (3)$$

where $P_L$ and $P_G$ are the liquid and gas pressures, respectively.

From the above analysis, the criteria for the existence of entrapped gas were only based on mechanical principle. For superhydrophobicity of a water drop on a surface, it is sufficient because the rolling of a drop is thermodynamically temporary. However, for evaluating the long-term stable existence of underwater entrapped gas, the above mechanical criteria are insufficient and some thermodynamic criteria, such as Eq. (1), should be met.

## 3 Drag reduction by gas

### 3.1 Drag reduction of superhydrophobic surface

Due to the much smaller viscosity of gas compared to water, superhydrophobic surfaces show a promising nature for passive drag reduction by entrapped gas. Due to the entrapped gas in the microstructures of a superhydrophobic surface, the liquid–gas interfaces replace partially the original liquid–solid interfaces, resulting in interfacial slippage, as shown in Fig. 6. The slippage induced by the entrapped gas is considered as a reason for the underwater drag reduction of the superhydrophobic surfaces. As shown in Fig. 7, a slip length is frequently used to gauge the slippery nature for reducing viscous drag. The flow velocity profile near the immersed surface is normally used to obtain the slip length for evaluating the viscous drag

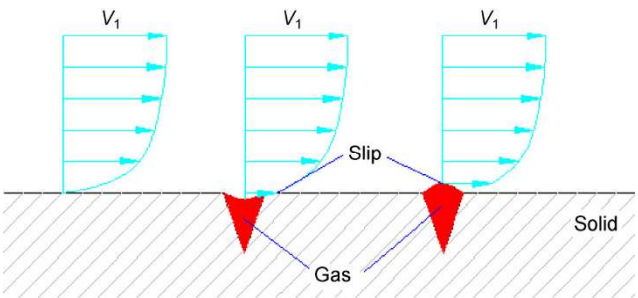


**Fig. 6** Schematic diagram of slip on the gas at a solid–liquid interface.

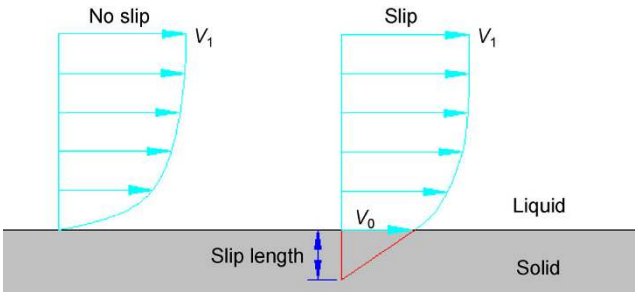


**Fig. 7** Schematic diagram of slip length.

reduction [68–71]. When a surface is hydrophilic, the measured velocity profile is consistent with the solution of Stokes' equation and well-accepted no-slip boundary condition. However, for a superhydrophobic surface, an apparent velocity slippage can be measured just above the solid surface [71].

Superhydrophobic surfaces can support a shear-free gas–water interface between surface topology peaks. The slip length of superhydrophobic surfaces has been proved in previous studies by measuring the velocity profile obtained by the particle image velocimetry (PIV) system [72] or laser Doppler velocimetry system [69]. Daniello et al. [69] measured the slip length to be 25 μm or more on a superhydrophobic surface using PIV. In the study, assuming that the total drag of the superhydrophobic surface was only determined by the viscous drag, a reduction rate of 50% was achieved.

Though the entrapped gas in the microstructures of a superhydrophobic surface can induce slippage, which can achieve the reduction of the viscous drag, the asperity peaks entrapping gas and the meniscus surfaces of the entrapped gas or bubbles can also induce a new extra pressure drag and a change of the slip nature. Rothstein determined that the geometrical variation of the bubbles on a solid surface had a significant effect on the fluid–solid interfacial slip and the drag reduction [73, 74]. Hyvaluom also determined that the slip length on the protruded bubbles decreased from a positive to negative value with decreasing water contact angle [75, 76]. Chen determined the friction force switched from decreasing to increasing as the bubbles grew on a solid surface [77]. Therefore, the total drag change is determined by simultaneously reducing the viscous drag by gas and increase of new extra pressure drag. The drag reduction is visible only when the reduction of the viscous drag is larger than that of the new extra pressure drag. Specifically, the measurement of slippage gauging the reduction of the viscous drag is insufficient for the total drag reduction by a superhydrophobic surface, and the total drag reduction should be measured. Aljallis et al. [78] conducted the measurement of skin friction drag by a mechanical transducer on superhydrophobic-coated flat plates in a high-speed towing tank. Compared to an uncoated bare aluminum plate, a significant drag reduction of up to 30% was observed on the superhydrophobic plate. Choi et al. [79] measured the torque applied to the rotating cone through a cone-and-plate rheometer for a plate with hydrophobic surface. Here, an average slip length of 20 μm in a water flow was calculated from the torque, which reflected the total drag reduction. In a pipeline flow, a flow rate under a constant shear stress value or same pressure difference between different pipelines could be used to evaluate the effect of drag reduction [34, 80]. Shirtcliffe et al. [34] presented experiments by this method to evaluate the drag reduction of a superhydrophobic inside surface of round copper tubes. The results showed that this type of surface allowed greater flow than that with smooth inside surface at low pressure difference. In addition, McHale et al. measured the terminal velocity of solid acrylic spheres with superhydrophobic surface settling under the action of gravity in water [81]; according to the terminal velocity, a drag reduction rate of approximately 25% was achieved.

Furthermore, considering the slippage at underwater liquid–gas interface, various roles of gas for drag reduction were theoretically investigated [32, 82, 83]. The numerical simulations of water flow beyond a superhydrophobic sphere with a lubricating air layer (plastron) were conducted using a two-phase flow representation; a drag reduction of up to 19% was achieved [84].

### 3.2 Drag reduction of other surfaces

The topography of superhydrophobic surfaces is homogeneous and mainly composed by diversities such as papilla preventing water from immersing the bottom of the surface asperities. In a flow field, an extra pressure drag is created by the entrapped gas in the microstructures of a superhydrophobic surface, and the entrapped gas is sheared along the flow direction and can be easily removed. Therefore, some heterogeneous surface structures were proposed to reduce the extra pressure drag and be against the shearing of the flow for sustaining the entrapped gas.

The longitudinal grooved surface can achieve drag reduction without inducing any extra pressure drag when the gas can be sustained in the surface structures. Choi et al. designed a hydrophobic grated surface with dense but deep longitudinal nanometer grooves

and a noticeable slip of 100–200 nm, corresponding to 20%–30% reduction of pressure drop observed in flow water [85]. The state of the entrapped gas and the drag reduction rate by longitudinal grooves mainly depended on the characteristics of the surface structures [86–90]. When the width of the microgrooves was enlarged, an increasing slip length was achieved because of the curvature variation of the water–gas meniscus. However, if the pitch-to-width ratio of the groove structure increased to a critical value, meniscus penetration into the cavity was observed [69, 91]. Though a longitudinal grooved hydrophobic surface can induce a viscous drag reduction without any extra pressure drag, the entrapped gas is unstable and can be easily removed because of the interfacial shearing being in identical direction with the grooves in a flow.

To enhance the stability of the entrapped gas, a transverse grooved surface can be employed to block the gas mechanically in the grooves when water perpendicularly flows over them. Evidently, for a transverse grooved surface, an extra pressure drag can be generated because of the transverse grooves, which adversely affects the total drag reduction. Therefore, a transverse grooved surface has rarely been employed for underwater drag reduction. However, when the grooved structure is optimized to minimize the extra pressure, a stable drag reduction can be achieved for a long time because the entrapped gas cannot be easily discharged from the surface. Wang et al. [92, 93] proved that a transverse grooved surface could achieve underwater drag reduction based on theoretical and experimental investigations; more than 10% drag reduction rate was achieved at an optimized surface structure.

## 4 Stability of gas in underwater surface structure

Although superhydrophobic and some other surfaces have the capability of holding air pockets in their surface microstructures and have demonstrated an effective slippage for underwater drag reduction, it is difficult to stably sustain air pockets for a long time, especially under conditions where liquid is flowing over the surface with high speed or a certain liquid pressure. No superhydrophobic surface was shown to demonstrate the underwater non-wetting properties in realistic conditions [94]. Based on mechanics and thermodynamics, once the mechanical or the thermodynamic equilibrium of the entrapped gas is disturbed, the entrapped gas will finally reduce or disappear. The most serious difficulty encountered in the current for underwater drag reduction by gas was the instability of entrapped gas.

Investigations on the stability of the entrapped gas of a superhydrophobic surface have mainly focused on transition between the Cassie (with entrapped gas) and Wenzel (without entrapped gas) states. The transition is determined by a mechanical equilibrium of the interface or an energy barrier between the different states from mechanics [45, 46]. The results from energy and force analysis show that the Cassie state is metastable, and the Wenzel state is globally stable [95]. Therefore, for a drop on a superhydrophobic surface, the transition from the Cassie to Wenzel state can occur easily through impacting, size decreasing, etc. [45, 46]. Moreover, the transition from the Wenzel to Cassie state is a challenge. When a superhydrophobic surface is immersed in water, the reverse transition is impossible despite placing some efforts. For instance, for a two-level (dual-scale) topography of a superhydrophobic surface, when water wetted the first scale topography and the entrapped gas was squeezed into the space among the second topography with increasing surrounding water pressure, the entrapped gas was restored from the squeezed gas through decreasing pressure [96]. However, when water wetted all surface, the entrapped gas could not be restored forever [96]. Basic mechanism on the loss of the entrapped gas by hydraulic pressure can be analyzed using Eq. (3). As per Eq. (3), the intruding angle increases with the liquid pressure of surrounding water. When the liquid pressure increases a critical value, the intruding angle will arrive at the maximum asperity slope angle of the surface, resulting in water wetting surface and loss of entrapped gas. Once the surface is completely wetted under a critical liquid pressure, the entrapped gas cannot be recovered through decreasing liquid pressure because of no gas source.

In addition, the force balance can be disturbed by shear stress at the liquid–gas interface in a flow field.

In general, only the force equilibrium in the direction perpendicular to the liquid–gas interface was considered in the criteria for the existence of entrapped gas such as Eqs. (2) and (3). The entrapped gas in the hydrophobic microstructures of a surface can also be partially or completely removed by the interfacial shear induced by flow, as shown in Fig. 8(a). In flowing water, higher flow velocities cause faster removal rates of the surface air layer [80, 97]. The disappearance of entrapped gas would cause declining drag reduction because of decreasing slippage. Govardhan et al. showed that the flow rate through a channel with inside superhydrophobic surface gradually decreased to a constant value ($Q_\infty$), as shown in Fig. 8(b) [80]. Aljallis et al. [78] reported the measurement of skin friction drag on superhydrophobic-coated flat plates in a flow with a speed of up to 9 m/s. A reduction in the significant initial drag was observed on a superhydrophobic plate, i.e., up to 30%. However, with increasing flow velocity, a rise in drag was observed, which was attributed to the morphology of the surface air layer and its depletion by high shear flow.

Except for the above reason, the stability of entrapped gas is also affected by the thermodynamic equilibrium. When a superhydrophobic surface is immersed in water, the initial entrapped gas in the surface microstructures is from air. As per Eq. (1), only when the radius of curvature of the liquid–gas interface is small enough, thermodynamic equilibrium can be maintained. Therefore, majority of initial entrapped gas would dissolve into water, especially in water with low dissolved gas concentration and high gas solubility limit. In addition, the dissolving speed is directly proportional to the gas solubility limit and inversely proportional to the gas concentration, as shown in Fig. 9 [94]. The gas solubility limit in water can be affected by hydraulic pressure. The higher the hydraulic pressure, the higher the gas solubility limit. Consequently, the higher the hydraulic pressure, the smaller the thermodynamic equilibrium radius of curvature of the liquid–gas interface in Eq. (1) and the shorter the longevity of the entrapped gas on an immersed superhydrophobic surface [98].

In summary, the stability of the entrapped gas in underwater surface structures is decided by mechanical and thermodynamical equilibriums. The entrapped gas in the microstructures of a surface is not globally stable and cannot be recovered if completely disappeared [94]. It will also decrease and become more and more unstable with increasing surrounding hydraulic pressure [94]. The majority of the entrapped gas on a superhydrophobic surface can be speedily removed by a flow [80, 97]. Some heterogeneous hydrophobic surface structures, such as span-wise structures or transverse grooved structures can be designed to hold the entrapped gas against the shearing of the water–gas interface by flow. The current investigations show that the large size of surface microstructures is beneficial to the drag reduction but not to the stability of the entrapped gas. From thermodynamics, the majority of the entrapped gas should dissolve into water in sufficient time; however, if the surface microstructures are small, some part of the entrapped gas can exist stably.

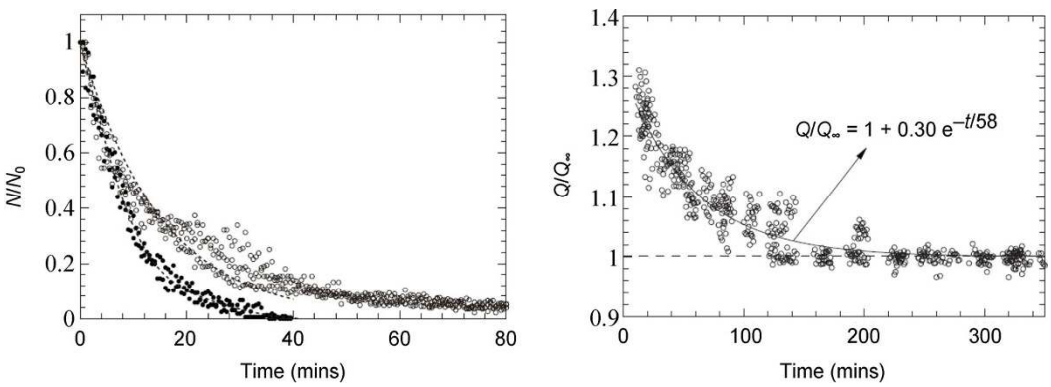


**Fig. 8** Time dependence of entrapped gas and drag reduction for hydrophobic surface immersed in water. (a) Variation of the number of trapped air pockets ($N$) seen in the direct visualization images with time. $N$ is normalized by the number of air pockets observed initially ($N_0$). (b) Time study of the flow rate required to maintain a constant value of shear stress. The channel is filled with water at $t = 0$, and the flow rate $Q$ required to maintain a constant value of shear stress is found to decrease with time and asymptote to a value $Q_\infty$ [80].

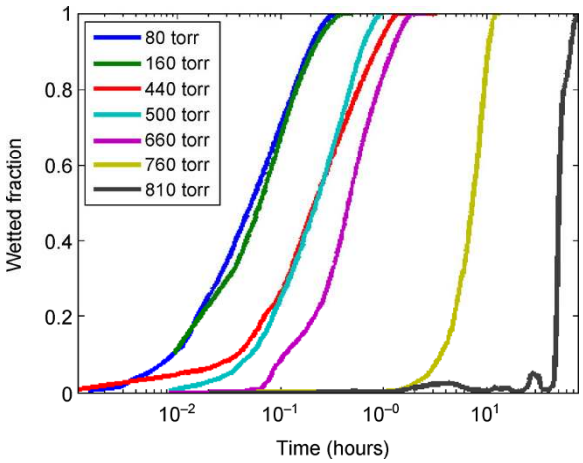


**Fig. 9** Thermodynamic longevity of entrapped gas in superhydrophobic surface structures in water of different initial dissolved gas concentrations. Here, different initial gas concentrations were achieved by different initial water equilibration and total dissolved gas pressures [94].

## 5 Gas supplement for drag reduction

From the above mechanical and thermodynamic analysis on the stability of gas at a water–solid interface, the initial entrapped gas is generally from air and is always easily removed in a flow field. Therefore, it is necessary to replenish a new gas supply for continued presence of gas at the interface for continued underwater drag reduction. There are two methods for gas supplement, i.e., active and passive.

### 5.1 Active gas supplement for drag reduction

Some active approaches have been tried to replenish the gas removed out from a surface. Gas injection is one of the simple and effective ways to achieve a lubricating gas film on an underwater solid surface [99, 100]. Elbing et al. [101] achieved drag reduction by injecting gas (air); a friction drag reduction larger than 80% was observed. The gas generation on a substrate was also achieved by water electrolysis or pyrolysis [102, 103]. Mccormick et al. proposed a method for creating hydrogen gas on a hull by electrolysis; a viscous drag reduction rate of approximately 10% was obtained [102]. Lee and Kim applied an additional electric field to achieve gas restoration after the entrapped gas disappeared by a liquid pressure [103]. Vakarelski et al. created a continuous and robust lubricating vapor layer on a surface by a thermal method of Leidenfrost effect; a drag reduction rate over 85% was achieved [104]. Although these active approaches achieved a substantial drag reduction, extra energy and some gas providing device were required, which limited their practical applications.

### 5.2 Passive gas generation for drag reduction

The possible methods for passive gas generation mainly include the precipitation of dissolved gas from water, supercavitation by low hydraulic pressure in water, and evaporation of a gas–water interface.

When water is initially supersaturated with dissolved gas, bubbles in water can thermodynamically grow due to the separation of dissolved gas from water [105–107]. Thermodynamics, however, does not tell us how long this process will take. In many cases, once gas solubility limit has been exceeded, nothing happens, i.e., the system becomes supersaturated, and (spontaneous) separation occurs only at some higher gas concentration or only after a very long time. Simultaneously, the separation speed of dissolved gas is very slow. The time for a gas bubble with 10 μm radius to grow up to 10 times in size is approximately several hundred seconds under the supersaturation of 25% relative to gas solubility limit [106]. Based on the mechanical analysis and investigations, the loss speed of the entrapped gas by a flow is much faster than the generation speed of gas by the precipitation of dissolved gas in water. Furthermore, when the dissolved gas concentration is less than the gas solubility limit, gas can only exist in a concave at a water–solid interface with a small curve radius. The precipitation of dissolved gas cannot happen subsequently for entrapped gas which has a larger size than the critical size in Eq. (1). Therefore, it is difficult to employ the precipitation of dissolved gas in water to generate gas for underwater drag reduction, resulting in non-application of this method.

Supercavitation is the use of cavitation effects to create a bubble in water, large enough to encompass an object traveling through water, significantly reducing the skin friction drag on the object. Cavitation occurs when water pressure is less than the saturated vapor pressure [108, 109], forming vapor bubbles. It can happen when water is accelerated to high speeds as when turning a sharp corner around a moving object

such as a ship's propeller or a pump's impeller. To create a bubble large enough to encompass a moving object for drag reduction, a high speed, generally more than one hundred meters per second, is required. In real applications, to employ supercavitation for drag reduction, rocket propulsion usually has to be used for sustained operation, such as the Russian VA-111 Shkval supercavitating torpedo [2]. In addition, this can be achieved temporarily by an underwater projectile fired or an airborne projectile impacting the water [110, 111]. Therefore, the current applications of supercavitation are mainly limited to projectiles or very fast torpedoes and some propellers.

Evaporation is a type of vaporization that occurs from a liquid surface into a vapor phase. For evaporation, vapor generation is due to breaking the balance of water–gas interface rather than creating a cavity in water. In flowing water, the velocity threshold required for evaporation at water–gas interface is much less than that required for natural cavitation [108]. Wang et al. [37] determined the evaporation at the water–gas or water–vapor interface over the entrapped gas in surface microstructures inside flowing water, which can sustainably generate vapor for the continued drag reduction, as shown in Fig. 10. In this method, as a necessary premise for evaporation at water–gas interface, the stable entrapped gas within the surface is essential to achieve gas renewal. Therefore, the surface structure should be designed to enhance the stability of the entrapped gas and avoid the disappearance of the entrapped gas. To hold the entrapped gas against the interfacial shear by flow, a transverse grooved structure on a hydrophobic surface was employed [37]; to counteract the effect of hydraulic pressure and thermodynamic dissolution, the micrometer size and trapezoid grooves with smaller bottom were used [37]. In Wang's experiments, the mechanism

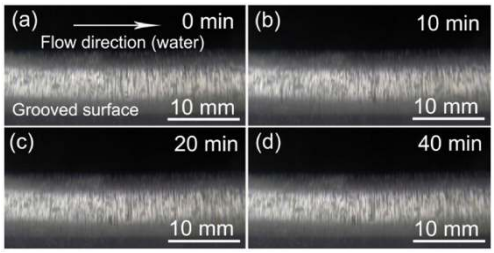


**Fig. 10** Image time sequence visualizing gases on the hydrophobic transverse microgrooved surface at the following different time intervals after immersion in water flowing at 5 m/s: (a) 0 (the starting time of the optical measurement), (b) 10 min, (c) 20 min, and (d) 40 min [37].

on the evaporation replenishing a new vapor supply for continued presence of vapor is still unclear, but it should be qualitatively attributed to the following factors: (1) low pressure of the entrapped gas because of Laplace pressure by the curved meniscus of the water–gas interface, as shown in Fig. 11(a), (2) high vapor density induced by forces of the solid surface such as van der Waals force near the three-phase point, as shown in Fig. 11(b), (3) interfacial stretching of the water–gas interface near the three-phase point by a process from the no-slip of the water–solid interface to the slip of the water–gas interface in a flow, as shown in Fig. 11(c), (4) the induction flow of the entrapped gas by the shearing of the water–gas interface in a flow, bringing vapor from high vapor density area to the other place, as shown in Fig. 11(d), and (5) low pressure and shear stress near the entrapped gas by flow.

If the hydrophobic grooved surface is immersed in static for a long time, the majority of the entrapped gas in grooves will thermodynamically dissolve in water or leave the grooves. However, thermodynamics also explains that a part of the entrapped gas can stably exist when the minimal radius of the grooves is less than the equilibrium critical radius in Eq. (1). Once some part of the entrapped gas exists, the

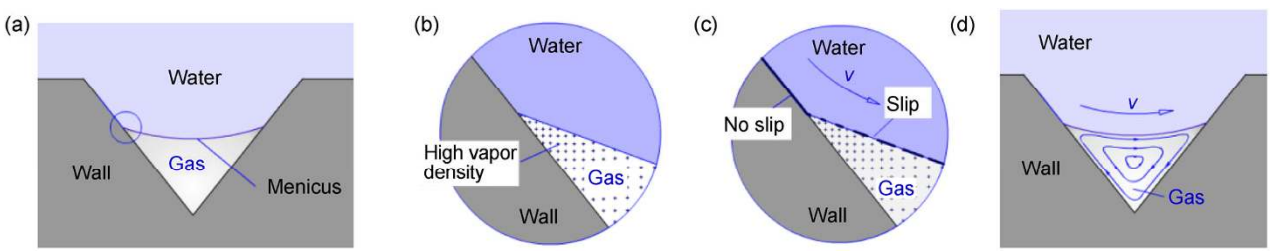


**Fig. 11** Schematic figures of the factors inducing evaporation to replenish a new vapor supply for continued presence of vapor in a groove: (a) cross-section of a groove, (b) and (c) enlarged figures of the circle section in (a), and (d) flow field of the entrapped gas.

evaporation can still happen when a flow is applied in water, resulting in the recovery of the entrapped gas and continued vapor generation for drag reduction. Till date, under the action of flowing, the gas generation by a hydrophobic transverse microgrooved surface was achieved at low flow velocity even at 1 m/s. Therefore, the evaporation induced by the liquid–gas interface can be considered as an excellent choice to achieve the renewal gas and future practical application because of its availability.

## 6 Summary

This paper presents a detailed analysis of our current understanding on underwater drag reduction by gas. It highlights the achievements and shortcomings of the current technologies. Combining the investigations, three critical points should be valuable for the underwater drag reduction researches:

(1) Entrapped gas is the key for underwater drag reduction. The stability of the entrapped gas at an underwater water–solid interface should be determined by thermodynamic and mechanical principles. Superhydrophobic state of a drop is induced by the entrapped gas in the surface microstructures and is a metastable state, referred as the Cassie state. The main cause for designing a superhydrophobic surface is to prevent water drop from immersing the bottom of the surface topography based on the interface mechanical analysis along the vertical direction without any thermodynamic requirements. Therefore, when a superhydrophobic surface is immersed with water, the entrapped gas in the underwater surface microstructures will be unstable because of the mechanical shearing of flow and the thermodynamic diffusion of the gas, resulting in non-practical application of superhydrophobic surfaces for underwater drag reduction. Though some heterogeneous surface structures were proposed to entrap gas against the shearing of the flow, majority of the entrapped gas will still disappear because of the thermodynamic diffusion.

(2) Entrapped gas in the microstructures of an underwater surface can induce an interface slippage, resulting in the reduction of the viscous drag. However, the surface asperities capturing gas and the meniscus surfaces of the entrapped gas can also induce a new extra pressure drag. Therefore, it should be simultaneously determined by the reduction of the viscous drag and the new extra pressure drag, whether or not the total drag reduction by the entrapped gas appears underwater.

(3) From thermodynamics and mechanics, majority of the entrapped gas at a water–solid interface should gradually disappear in a flow field. Therefore, the replenishment of gas supplement is essential for continued presence of gas and underwater drag reduction. Compared with other methods for gas generation, the evaporation induced by liquid–gas interface over the entrapped gas can be considered as an excellent choice to achieve the renewal gas and future practical application.

## Acknowledgement

This work was supported by the National Natural Science Foundation of China (Grant Nos. 51375253, and 51321092).



## References

[1] Shi X H, Wang X J. *Introduction to Underwater Weapon* (*Torpedo*). Xi'an: Northwestern Polytechnical University Press, 1995: 28–33.

[2] Ke G X, Pan G, Huang Q G, Hu H B, Liu Z Y. Review of underwater drag reduction technology. *Adv Mech* **39**: 546–554 (2009)

[3] Jiang C G, Xin S C, Wu C W. Drag reduction of a miniature boat with superhydrophobic grille bottom. *AIP Adv* **1**: 032148 (2011)

[4] Zhang D Y, Li Y Y, Han X, Li X, Chen H W. High-precision bio-replication of synthetic drag reduction shark skin. *Chinese Sci Bull* **56**: 938–944 (2011)

[5] Wang B, Wang J D, Zhou G, Chen D R. Drag reduction by micro vortexes in transverse microgrooves. *Adv Mech Eng* **2014**: 734012 (2014)

[6] Mei D J, Fan B C, Chen Y H, Ye J F. Experimental

investigation on turbulent channel flow utilizing spanwise oscillating Lorentz force. *Acta Phys Sin* **59**: 8335–8342 (2010)

[7] Li G, Li S M, Xu Y J, Zhang Y, Li HM, Nie CQ, Zhu J Q. Experimental study of near wall region flow control by dielectric barrier discharge plasma. *Acta Phys Sin* **58**: 4026–4033 (2009)

[8] Walsh M J. Riblets as a viscous drag reduction technique. *AIAA J* **21**: 485–486 (1983)

[9] Choi J, Jeon W P, Choi H. Mechanism of drag reduction by dimples on a sphere. *Phys Fluids* **18**: 041702 (2006)

[10] García-Mayoral R, Jiménez J. Drag reduction by riblets. *Phil Trans R Soc A* **369**: 1412–1427 (2011)

[11] Ranjan P, Ranjan A R, Singh A P. Computational analysis of frictional drag over transverse grooved flat plates. *Int J Eng Sci Tech* **3**: 110–116 (2011)

[12] Wang X N, Gen X G, Zang D Y. Drag-reduction of one-dimensional period and puasiperiod groove structures. *Acta Phys Sin* **62**: 4701 (2013)

[13] Li F C, Cai W H, Zhang H N, Wang Y. Influence of polymer additives on turbulent energy cascading in forced homogeneous isotropic turbulence studied by direct numerical simulations. *Chin Phys B* **21**: 114701 (2012)

[14] Mowla D, Naderi A. Experimental study of drag reduction by a polymeric additive in slug two-phase flow of crude oil and air in horizontal pipes. *Chem Eng Sci* **61**: 1549–1554 (2006)

[15] Yang S Q, Dou G. Turbulent drag reduction with polymer additive in rough pipes. *J Fluid Mech* **642**: 279–294 (2010)

[16] Li F C, Kawaguchi Y, Yu B, Wei J J, Hishida K. Experimental study of drag-reduction mechanism for a dilute surfactant solution flow. *Int J Heat Mass Tran* **51**: 835–843 (2008)

[17] Yao Y, Lu C-J, Si T. Water tunnel experimental investigation on the drag reduction characteristics of the traveling wavy wall. *J Hydrodynamics* **23**(1): 65–70 (2011)

[18] Walsh M J, Lindemann A M. Optimization and application of riblets for turbulent drag reduction. American Institute of Aeronautics and Astronautics. *AIAA Paper* **84**: 0347 (1984)

[19] Wilkinson S P, Lazos B S. Turbulent viscous drag reduction with thin-element riblets. *AIAA J* **26**: 496–498 (1988)

[20] Walsh M J. Effect of detailed surface geometry on riblet drag reduction performance. *Aircraft* **27**: 572 (1990)

[21] Neumann D, Dinkelacker A. Drag measurements on V-grooved surfaces on a body of revolution in axial flow. *Appl Sci Res* **48**: 105 (1991)

[22] Rohr J J, Andersen G W, Reidy L W, Hendricks E W. A comparison of the drag-reducing benefits of riblets in internal and external flows. *Exp Fluids* **13**: 361 (1992)

[23] Bechert D W, Bruse M, Hage W, van der Hoeven J G T, Hoppe G. Experiments on drag-reducing surfaces and their optimization with an adjustable geometry. *J Fluid Mech* **338**: 59–87 (1997)

[24] Bechert D W, Bruse M, Hage W. Experiments with three-dimensional riblets as an idealized model of shark skin. *Exp Fluids* **28**: 403 (2000)

[25] Ghazali N N N, Yau Y H, Badarudin A, Lim Y C. Computational fluid dynamics (CFD) simulation of drag reduction by riblets on automobile. *AIP Publishing* **1233**(1): 1535–1540 (2010)

[26] Buttner C C, Schulz U. Shark skin inspired riblet coatings for aerodynamically optimized high temperature. *Applications in Aeroengines* **20**: 1 (2011)

[27] García-Mayoral R, Jiménez J. Scaling of turbulent structures in riblet channels up to Reτ ≈ 550. *Phys Fluids* **24**(10): 105101 (2012)

[28] Gad-el-Hak M. Interactive control of turbulent boundary layers: A futuristic overview. *AIAA J* **32**: 1753–1765 (1994)

[29] Kasliwal A, Duncan S, Papachristodoulou A. Modelling channel flow over riblets: Calculating the energy amplification. In *Proc. IEEE UKACC International Conference on Control*, 2012: 625–630.

[30] Lang A, Motta P, Habegger M L, Hueter R. In *Shark Skin boundary Layer Control/ Natural Locomotion in Fluids and on Surfaces*. New York: Springer, 2012: 139–150.

[31] Meysonnat P, Klumpp S, Meinke M, Schroder W. Variation of friction drag via spanwise transversal surface waves. *PAMM* **12**: 575–576 (2012)

[32] Martell M B, Rothstein J P, Perot J B. An analysis of superhydrophobic turbulent drag reduction mechanisms using direct numerical simulation. *Phys Fluids* **22**: 065102 (2010)

[33] Martell M B, Perot J B, Rothstein J P. Direct numerical simulations of turbulent flows over superhydrophobic surfaces. *J Fluid Mech* **620**: 31–41 (2009)

[34] Shirtcliffe N J, McHale G, Newton M I, Zhang Y. Superhydrophobic copper tubes with possible flow enhancement and drag reduction. *ACS Appl Mater Inter* **1**: 1316–1323 (2009)

[35] Sugiyama. K, Calzavarini. E, Lohse D. Microbubbly drag reduction in Taylor–Couette flow in the wavy vortex regime. *J Fluid Mech* **608**: 21–42 (2008)

[36] Lee C, Kim C J. Wetting and active dewetting processes of hierarchically constructed superhydrophobic surfaces fully immersed in water. *Journal of Microelectromechanical Systems* **21**: 712–720 (2012)

[37] Wang B, Wang J D, Chen D R. Continual automatic

generation of gases on hydrophobic transverse microrooved surface. *Chem Lett* **43**(5): 646–648 (2014)

[38] Zhang X H, Maeda N, Craig V S J. Physical properties of nanobubbles on hydrophobic surfaces in water and aqueous solutions. *Langmuir* **22**(11): 5025–5035 (2006)

[39] Ishida N, Inoue T, Miyahara M. Nano bubbles on a hydrophobic surface in water observed by tapping-mode atomic force microscopy. *Langmuir* **16**(16): 6377–6380 (2000)

[40] Yang JW, Duan J, Fornasiero D, and Ralston J. Very small bubble formation at the solid-water interface/contact angle and stability of interfacial nanobubbles. *J Phys Chem B* **107**: 6139–6147 (2003)

[41] Zhang X H, Quinn A, Ducker W A. Nanobubbles at the interface between water and a hydrophobic solid. *Langmuir* **24**(9): 4756–4764 (2008)

[42] Li J, Chen H S. Growth of bubbles on a solid surface in response to a pressure reduction. *Langmuir* **30**: 4223–4228 (2014)

[43] Wang J, Chen H, Sui T, Chen D R. Investigation on hydrophobicity of lotus leaf: Experiment and theory. *Plant Sci* **176**(5): 687–695 (2009)

[44] Barbieri L, Wagne E, Hoffmann P. Water wetting transition parameters of perfluorinated substrates with periodically distributed flat-top microscale obstacles. *Langmuir* **23**(4): 1723–1734 (2014)

[45] Extrand C W. Criteria for ultralyophobic surfaces. *Langmuir* **20**(12): 5013–5018 (2004)

[46] Wang J D, Chen D R. Criteria for entrapped gas under a drop on an ultrahydrophobic surface. *Langmuir* **24**: 10174–10180 (2008)

[47] Gao X F, Jiang L. Water-repellent legs of water striders. *Narture* **432**: 36–37(2004)

[48] Ren L Q. Progress in the bionic study on anti-adhesion and resistance reduction of terrain machines. *Sci Chin Tech Sci* **52**: 273–284 (2009)

[49] Dai Z D, Tong J, Ren L Q. Researches and developments of biomimetics in tribology. *Chinese Sci Bull* **51**: 2681–2689 (2006)

[50] Neinhuis C, Barthlott W. Characterization and distribution of water-repellent, self-cleaning plant surfaces. *Ann Bot* **79**: 667–677 (1997)

[51] Bixler G D, Bhushan B. Bioinspired rice leaf and butterfly wing surface structures combining shark skin and lotus effects. *Soft Matter* **8**: 11271–11284 (2012)

[52] Bhushan B. Bioinspired structured surfaces. *Langmuir* **28**: 1698–1714 (2012)

[53] Fang Y, Sun G, Cong Q, Chen G H, Ren L Q. Effects of methanol on wettability of the non-smooth surface on butterfly wing. *J Bonic Eng* **5**: 127–133 (2008)

[54] Yao J, Wang J N, Yu Y H, Yang H, Xu Y. Biomimetic fabrication and characterization of an artificial rice leaf surface with anisotropic wetting. *Chinese Sci Bull* **57**: 2631–2634 (2012)

[55] Fang Y, Sun G, Wang T Q, Cong Q, Ren L Q. Hydrophobicity mechanism of non-smooth pattern on surface of butterfly wing. *Chinese Sci Bull* **52**: 711–716 (2007)

[56] Gogte S, Vorobieff P, Truesdell R, Mammoli A, Van Swol F, Brinker C J. Effective slip on textured superhydrophobic surfaces. *Phys Fluids* **17**: 51701 (2005)

[57] Wenzel R N. Resistance of solid surfaces to wetting by water. *Ind Eng Chem* **28**: 988 (1936)

[58] Cassie A B D,Baxter S. Wettability of porous surfaces. *Trans Faraday Soc* **40**: 546 (1944)

[59] McHale G, Newton M I, Shirtcliffe N J. Immersed superhydrophobic surfaces: Gas exchange, slip and drag reduction properties. *Soft Matter* **6**: 714–719 (2010)

[60] Maali A, Pan Y, Bhushan B, Charlaix E. Hydrodynamic drag-force measurement and slip length on microstructured surfaces. *Phys Rev E* **85**: 066310 (2012)

[61] Larmour I A, Bell S E J, Saunders G C. Remarkably simple fabrication of superhydrophobic surfaces using electroless galvanic deposition. *Angew Chem* **119**: 1740–1742 (2007)

[62] Sakai M, Yanagisawa T, Nakajima A, Kameshima Y, Okada K. Effect of surface structure on the sustainability of an air layer on superhydrophobic coatings in a water–ethanol mixture. *Langmuir* **25**: 13–16 (2008)

[63] Sakai M, Nakajima A, Fujishima A. Removing an air layer from a superhydrophobic surface in flowing water. *Chem Lett* **39**: 482–484 (2010)

[64] Poetes R, Holtzmann K, Franze K, Steiner U. Metastable underwater superhydrophobicity. *Phys Rev Lett* **105**: 166104 (2010)

[65] Scardino A J, Zhang H, Cookson D J, Lamb R N, de Nys R. The role of nano-roughness in antifouling. *Biofouling* **25**: 757–767 (2009)

[66] Lee C, Choi C H. Structured surfaces for a giant liquid slip. *Phys Rev Lett* **101**: 064501(2008)

[67] Lee C, Kim C J. Maximizing the giant liquid slip on superhydrophobic microstructures by nanostructuring their sidewalls. *Langmuir* **25**: 12812–12818 (2009)

[68] Maali A, Bhushan B. Measurement of slip length on superhydrophobic surfaces. *Philos T R Soc A* **370**: 2304–2320 (2012)

[69] Daniello R J, Waterhouse N E, Rothstein J P. Drag reduction in turbulent flows over superhydrophobic surfaces. *Phys Fluids* **21**: 085103 (2009)

[70] Tretheway D C, Meinhart C D. Apparent fluid slip at hydrophobic microchannel walls. *Phys Fluids* **14**: L9 (2002)

[71] Byun D, Kim J, Ko H S, Hoon C P. Direct measurement of slip flows in superhydrophobic microchannels with transverse grooves. *Phys Fluids* **20**: 113601 (2008)

[72] Sakai M, Nishimura M, Morii Y, Furuta T, Lsobe T, Fujishima A, Nakajima A. Reduction of fluid friction on the surface coated with $TiO_2$ photocatalyst under UV illumination. *J Mat Sci* **47**: 8167–8173 (2012)

[73] Quere D. Wetting and roughness. *Annu Rev Mater Res* **38**: 71–99 (2008)

[74] Rothstein J P. Slip on superhydrophobic surfaces. *Annu Rev Fluid Mech* **42**: 89−109 (2010)

[75] Steinberger A, Cottin-Bizonne C, Kleimann P, Charlaix E. High friction on a bubble mattress. *Nat Mater* **6**: 665–668 (2007)

[76] Hyvaluoma J, Harting J. Slip flow over structured surfaces with entrapped microbubbles. *Phys Rev Lett* **100**: 246001 (2008)

[77] Chen H, Li J, Chen D. Study of drag forces on a designed surface in bubbly water lubrication using electrolysis. *J Fluids Eng─Trans ASME* **128**: 1383–1389 (2006)

[78] Aljallis E, Sarshar M A, Datla R, Sikka V, Jones A, Choi C H. Experimental study of skin friction drag reduction on superhydrophobic flat plates in high Reynolds number boundary layer flow. *Phys Fluids* **25**: 025103 (2013)

[79] Choi C H, Kim C J. Large slip of aqueous liquid flow over a nanoengineered superhydrophobic surface. *Phys Rev Lett* **96**: 066001 (2006)

[80] Govardhan R N, Srinivas G S, Asthana A, Bobji M S. Time dependence of effective slip on textured hydrophobic surfaces. *Phys Fluids* **21**: 052001 (2009)

[81] McHale G, Shirtcliffe N J, Evans C R, Newton M I. Terminal velocity and drag reduction measurements on superhydrophobic spheres. *Appl Phys Lett* **94**: 064104 (2009)

[82] McHale G, Flynn M R, Newton M I. Plastron induced drag reduction and increased slip on a superhydrophobic sphere. *Soft Matter* **7**: 10100–10107 (2011)

[83] Cao L, Wu J, Gao D. Reynolds number dependence of drag reduction and interfacial slip over superhydrophobic surfaces. *Adv Sci Eng Med* **4**: 345–349 (2012)

[84] Gruncell B R K, Sandham N D, McHale G. Simulations of laminar flow past a superhydrophobic sphere with drag reduction and separation delay. *Phys Fluids* **25**: 043601 (2013)

[85] Choi C H, Ulmanella U, Kim J, Ho C M, Kim C J. Effective slip and friction reduction in nanograted superhydrophobic microchannels. *Phys Fluids* **18**: 087105 (2006)

[86] Kwon B H, Kim H H, Park K, Park J H, Choi D G, Go J S. Frictional drag reduction in microchannel using slip on convex air bubbles naturally formed in a specifed a cavity. In *Proc. IEEE 16th International Solid-State Sensors, Actuators and Microsystems Conference (TRANSDUCERS)* 2011: 1288–1291.

[87] Luu L H, Forterre Y. Giant drag reduction in complex fluid drops on rough hydrophobic surfaces. *Phys Rev Lett* **110**: 184501 (2013)

[88] Cottin-Bizonne C, Barrat J L, Bocquet L, Charlaix E. Low-friction flows of liquid at nanopatterned interfaces. *Nature Mater* **2**: 237–240 (2003)

[89] Wang J D, Yu Y, Chen D R. Research progress on the ultra hydrophobic surface topography effect. *Chinese Sci Bull* **51**: 2297–2300 (2006)

[90] Zheng LJ, Wu XD, Luo Z, Wu D. Superhydrophobicity from microstructured surface. *Chinese Sci Bull* **49**: 1779–1787 (2004)

[91] Tsai P, Peters A M, Pirat C, Wessling M, Lammertink R G H, Lohse D. Quantifying effective slip length over micro-patterned hydrophobic surfaces. *Phys Fluids* **21**: 112002 (2009)

[92] Wang B, Wang J D, Chen D R. A prediction of drag reduction by entrapped gases in hydrophobic transverse grooves. *Sci Chin Tech Sci* **56**: 2973–2978 (2013)

[93] Wang B, Wang J D, Chen D R. Drag reduction on hydrophobic transverse grooved surface by gas naturally formed under-water. *Acta Phys Sin* **63**: 074702 (2014)

[94] Sun W Y, Kim C J. The role of dissolved gas in longevity of Cassie states for immersed superhydrophobic surfaces. In *Proc. IEEE 26th International Conference on Micro Electro Mechanical Systems (MEMS)*, 2013: 397–400.

[95] Giacomello A, Meloni S, Chinappi M, Casciola C M. Cassie–Baxter and Wenzel states on a nanostructured surface: Phase diagram, metastabilities, and transition mechanism by atomistic free energy calculations. *Langmuir* **28**:10764–10772 (2012)

[96] Verho T, Korhonen J T, Sainiemi L, Jokinen V, Franze K, Franssila S, Andrew P, Ikkala O, Ras R H A. Reversible switching between superhydrophobic states on a hierarchically structured surface. *Proc Natl Acad Sci USA* **109**: 10210–10213 (2012)

[97] Karatay E, Haase A S, Visser C W, Sun C, Lohse D, Tsai P A, and Lammertink R G H. Control of slippage with tunable bubble mattresses. *Proc Natl Acad Sci USA* **110**: 8422–8426 (2013)

[98] Forsberg P, Nikolajeff F, Karlsson M. Cassie–Wenzel and Wenzel–Cassie transitions on immersed superhydrophobic

surfaces under hydrostatic pressure. *Soft Matter* **7**: 104–109 (2011)

[99] Sayyaadi H, Nematollahi M. Determination of optimum injection flow rate to achieve maximum micro bubble drag reduction in ships; an experimental approach. *Sci Iran* **20**: 535–541 (2013)

[100] Lauga E, Stone H A. Effective slip in pressure-driven Stokes flow. *J Fluid Mech* **489**: 55–77 (2003)

[101] Elbing B R, Winkel E S, Lay K A, Ceccio S L, Dowling D R, Perlin M. Bubble-induced skin-friction drag reduction and the abrupt transition to air-layer drag reduction. *J Fluid Mech* **612**: 201–236 (2008)

[102] Mccormick M E, Bhattacharyya R. Drag reduction of a submersible hull by electrolysis. *Naval Eng J* **85**: 11–16 (1973)

[103] Lee C, Kim C J. Underwater restoration and retention of gases on superhydrophobic surfaces for drag reduction. *Phys Rev Lett* **106**: 014502 (2011)

[104] Vakarelski I U, Marston J O, Chan D Y C, Thoroddsen S T. Drag reduction by Leidenfrost vapor layers. *Phys Rev Lett* **106**: 214501(2011)

[105] Kim W T, Cho Y I. A study of scale formation around air bubble attached on a heat-transfer surface. *Inter Commun Heat Mass* **29**: 1–14 (2002)

[106] Kwak H Y, Kim Y W. Homogeneous nucleation and macroscopic growth of gas bubble in organic solutions. *Inter J Heat Mass Transfer* **41**(4): 757–767 (1998)

[107] Epstein P S, Plesset M S. On the stability of gas bubbles in liquid–gas solutions. *J Chem Phys* **18**: 1505 (1950)

[108] Joseph D D. Cavitation and the state of stress in a flowing liquid. *J Fluid Mech* **366**: 367–378 (1998)

[109] Mohammadi A, Floryan J M. Pressure losses in grooved channels. *J Fluid Mech* **725**: 23–54 (2013)

[110] Choi J H, Penmetsa R C, Grandhi R V. Shape optimization of the cavitator for a supercavitating torpedo. *Struct Multidisc Optim* **29**: 159–167 (2005)

[111] Alyanak E, Venkayya V, Grandhi R, Penmetsa R. Structural response and optimization of a supercavitating torpedo. *Finite Elem Anal Des* **41**:563–582 (2005)

Jiadao WANG. He received his MS and Ph.D degrees in Mechanical Engineering from Tsinghua University, China, in 1996 and 2000 respectively. He is currently a professor in State Key Laboratory of Tribology at Tsinghua University. He joined the faculty at State Key Laboratory of Tribology of Tsinghua University in 1999. His research interests include interface forces and surface engineering.